P2-80

Simulations of diffusive lithium evaporation onto the NSTX vessel walls

D. P. Stotler [a,*], C. H. Skinner [a], W. R. Blanchard [a],

P. S. Krstic [b] H. W. Kugel [a], H. Schneider [a], L. E. Zakharov [a],

[a] *Princeton Plasma Physics Laboratory, Princeton University, P. O. Box 451, Princeton, NJ 08543-0451, USA*

[b] *Oak Ridge National Laboratory, Oak Ridge, TN 37831, USA*

Abstract

A model for simulating the diffusive evaporation of lithium into a helium filled NSTX vacuum vessel is described and validated against an initial set of deposition experiments. The DEGAS 2 based model consists of a three-dimensional representation of the vacuum vessel, the elastic scattering process, and a kinetic description of the evaporated atoms. Additional assumptions are required to account for deuterium out-gassing during the validation experiments. The model agrees with the data over a range of pressures to within the estimated uncertainties. Suggestions are made for more discriminating experiments that will lead to an improved model.

Key words: (PSI-19), NSTX, Lithium, Coating, DEGAS, (JNM) T0100 Theory

and Modeling, L0300 Lithium

PACS: 81.15.-z, 34.50.-s, 52.65.Pp, 51.10.+y

1 Introduction

The National Spherical Torus eXperiment (NSTX, $R = 0.85$ m, $a < 0.67$ m, $R/a > 1.27$) [1] has been investigating the use of lithium as a surface coating material to improve plasma performance and to provide better control of the core plasma density. In the principal technique used thus far, lithium is evaporated from the top of the vessel via one or two evaporators (LITERs) [2] into a vacuum between discharges and is primarily deposited on the lower divertor surfaces. Lithium coatings have reduced deuterium recycling, improved confinement and suppressed ELMs [2,3,4]. However, in plasmas with suppressed ELMs, core carbon and medium-Z metallic impurity concentrations increase in the latter part of the discharge [4]. The temporal and spatial origin of these impurities is the subject of ongoing research, as is the search for techniques to prevent them being generated or to expel them periodically. The preventive technique that we consider here is to increase the coverage of the vacuum vessel with lithium so as to reduce sputtering of impurities from the graphite tiles and metal surfaces.

* Corresponding and presenting author
Email address: dstotler@pppl.gov (D. P. Stotler).

Evaporation into a helium filled vessel accomplishes this objective via diffusion of the lithium throughout the vessel. Observations of this effect were reported previously in conjunction with evaporation during helium glow discharge cleaning [5]. The mean free path of the lithium atoms scales inversely with the helium pressure, so lower pressures coat the bottom of the vessel most effectively and higher pressures lead to thicker coatings closer to the injectors at the top of the vessel. Because of the three dimensional (3-D) nature of the problem, an optimal strategy that provides a specified minimum coating thickness on all surfaces in the minimum amount of time, and with the least amount of lithium, is far from obvious. To this end, we have developed a model of this system using the 3-D Monte Carlo neutral transport code DEGAS 2 [6] that can be run multiple times for different helium pressures. The resulting lithium fluxes to the various plasma facing components are then used to compile an optimized coating procedure as a set of evaporation intervals at specified pressures.

This paper describes the initial validation of this model against diffusive evaporation experiments performed during the 2009 NSTX run campaign.

2 Model and Experimental Configuration

The first component of the simulation model is a 3-D description of the NSTX vacuum vessel, including the two LITER evaporators used in this run campaign, as well as a surface representing the quartz micro-balance (QMB) [5] that provides the deposition data with which the model is compared.

Coordinates for most tile surfaces have been taken from engineering drawings produced during the design and construction of NSTX. In-vessel measurements made during the most recent opening of NSTX provide updated coordinates for the lower divertor tile surfaces and the crucial toroidal gaps in front of the LITER evaporators and the QMB. The toroidal variation of the model, e.g, gaps between tiles, is prescribed in DEGAS 2 with a "pie slice" method [6] in which the various structures are represented as plane figures (Fig. 1) revolved about the major axis of the torus through a range of toroidal angles (Fig. 2). This toroidal discretization need not be uniform and is adapted to provide the appropriate toroidal widths for material surfaces. The LITERs are located at toroidal angles of 45° (Bay K) and 195° (Bay F). The QMB is at 225° (Bay E).

The angular distribution of lithium atoms emitted by the LITERs measured in the laboratory [2] agrees well with a molecular flow calculation [7] made using the Cbebm code. A spline fit to the latter forms the basis for the angular distribution

of the lithium source in DEGAS 2; the atoms have a thermal energy distribution with a temperature of 900 K. The LITERs are operated at a computer controlled temperature [2], and the corresponding evaporation rates are determined from the lithium vapor pressure and a molecular flow conductance calculation. Laboratory data confirm the accuracy of these rates. For the experiments described here, the LITERs were operated at $\sim$ 910 K with a corresponding evaporation rate of 60 mg/min.

The atomic physics processes in the problem are elastic scattering of lithium atoms off of helium and deuterium molecules. The latter enter as a result of significant out-gassing during the evaporation process. The relative amounts of helium and deuterium in the vessel will be discussed in Sec. 3.1. The differences between the mean free paths for the two processes, given in [5], are smaller than the uncertainties in either. If we assume, in the interest of simplicity, that they are the same, we can treat the two background species (He and D_2) as one by virtue of their equal masses and temperatures. The simulated pressure is then just the sum of the helium and deuterium pressures. We assume that this pressure is uniform throughout the vessel and at room temperature (300 K). The cross section used is that of the Li-He scattering as obtained by Hamel [8], $\sigma_{\mathrm{Li-He}} = 2.49 \times 10^{-19}$ m^2; the associated mean free path is

$$\lambda_{\mathrm{Li-He}} = 9.92 \times 10^{-2}/P_{\mathrm{tot}} \text{ m}, \tag{1}$$

where the pressure $P_{\rm tot}$ is in mtorr.

The final component of the model is the assumption that the lithium atoms stick to all materials surfaces inside the vacuum vessel with 100% probability or, equivalently, that all surfaces have the same sticking probability.

3 Experimental Data

The experiments providing the data for this paper were based on an initial pressure prescription for coating the vessel developed from an earlier set of DEGAS 2 simulations. The lowest pressure, 0.032 mtorr ($\lambda_{\rm Li-He} = 3.1$ m), provides the best coverage of the lower divertor and other surfaces near the bottom of the vessel. The highest pressure, 0.2 mtorr ($\lambda_{\rm Li-He} = 0.5$ m) coats the upper surfaces, although it also results in strong deposition peaks on the upper divertor plates around the LITERs. An intermediate pressure, 0.1 mtorr ($\lambda_{\rm Li-He} = 1.0$ m) is used to cover the midplane region and the primary passive plates. Apart from peaks in the coating thickness around the upper divertor, the largest departure from toroidal uniformity is on the portion of the lower center stack that is partially shadowed from both LITERs. This prescription has evaporation being performed at the lowest helium pressure for one unit of time and at the two higher pressures for two units of time each. For this experiment, the total evaporation time was selected to enable several

shots to be run during the time allotted to the experiment rather than to achieve a specified lithium thickness.

The practical implementation of this evaporation prescription begins with a 2.5 mtorr helium gas fill (normally used for glow discharge cleaning). The torus pumping system was then employed to bring the pressure down to 0.2 mtorr; at the same time, the LITER evaporation began. The vessel pressure rose during this interval due to out-gassing. Although the mass 2 (H_2, D) and 4 (D_2, He) signals from the residual gas analyzer were saturated for most of these evaporations, an examination of those from other NSTX experiments indicates that this gas is predominantly molecular hydrogen; we assume here that it is all D_2.

The pumps were turned on again at the completion of this evaporation interval to bring the vessel pressure down to 0.1 mtorr for the second evaporation period. We anticipated running the third evaporation interval at 0.03 mtorr in the same manner. However, the pressure rise from the out-gassing quickly exceeded that target pressure in the two initial experiments. On the subsequent three experiments, the torus pumps were left open during the third evaporation interval.

3.1 Pressure and QMB Data

The vessel pressures were measured by an ionization gauge. Being calibrated such that its readings provide the pressure of air, a calibration factor must be applied to obtain the pressure of other gases. For D_2, this is $c_{D_2} = 0.392$; for He, $c_{He} = 0.186$. Namely, we write the ionization gauge pressure as:

$$P_{ig} = c_{He} P_{He} + c_{D_2} P_{D_2}. \tag{2}$$

Having no other means of determining the precise composition of the gas at a given point in time, we assume that after pump-down of the initial prefill, the gas is all He. We then suppose that all pressure rise is due to out-gassing of D_2 and that the gas composition remains fixed during the subsequent pumping intervals. These assumptions together with Eq. (2) are sufficient to allow P_{He}, P_{D_2}, and $P_{tot} = P_{He} + P_{D_2}$ to be uniquely determined. The resulting pressures for the first of the five evaporation experiments are shown together with the target helium pressures in Fig. 3.

The operation of the QMB monitors is described in [9], [10] and [5]. The raw data from the monitors is a frequency that is directly proportional to deposited mass once the effects of temperature changes have been taken into account. If the deposits are all of the same atomic mass, this mass can be directly converted to a number of atoms or molecules and then into a deposition rate (or flux, by dividing

by the area of the monitor, 1.0×10^{-4} m^2). However, to facilitate interpretation the deposited mass is usually converted to a thickness using a nominal density of 1.6 gm/cm^3 [9], as in Fig. 3. Note that because this QMB is at the top of the vessel and relatively close to the Bay F LITER, the deposition rate is greatest at the highest pressures.

To compute that rate, the QMB data are first smoothed using a boxcar average 15 data points wide (about 1 minute). These data are then interpolated onto a time grid having a uniform spacing of 36 seconds, and the rate is computed by a finite difference derivative. The full set of experimental rates, divided by the LITER evaporation rate, is plotted as a function of the inferred total pressure in Fig. 4 under the assumption that the material deposited on the QMB is pure lithium. This normalized deposition rate is essentially the probability for an evaporated lithium atom to be deposited on the QMB. The "tracks" apparent in the data represent the trajectories of individual evaporation sequences, suggesting the presence of a missing parameter or systematic error, e.g., in the unfolding of the pressure data.

Another possible explanation of these variations in deposition rate at a given pressure is that the material accumulated on the QMB is not pure lithium, but is of varying chemical composition. In particular, the mass 18 signals from the residual gas analyzer indicate that the out-gassing contains in excess of 10^{-6} torr of water. While these water molecules will not result in significant scattering of lithium

atoms in the vessel, they may hydrate the lithium as it is being deposited on the QMB surface. For example, 10^{-6} torr of water results in a flux of H_2O to the QMB surface an order of magnitude larger than the largest lithium fluxes considered here. In the limit that all of the deposited lithium is being hydrated, the mass to be used in computing the deposition rate is that of LiOH. In the next section, we will assume that the effective mass of the deposited material lies somewhere between the extremes of pure Li and pure LiOH. Note that the presence of water in the vessel during evaporation does not necessarily result in passivation of lithium deposited on graphite surfaces [11].

A related effect is that nonuniformities in the deposits can lead to mechanical stresses and consequent changes in the observed QMB frequency [5]. Since such effects would enter intermittently or gradually over intervals longer than those considered here, we neglect them.

4 Simulations and Analysis

A set of simulations has been done at 0.032, 0.1, 0.25, and 0.3 mtorr for the purpose of comparing with these data. The resulting "baseline" normalized deposition rates are plotted in Fig. 4.

The uncertainty in the depth of the QMB below the secondary passive plates is

estimated to be 1 cm. The corresponding variation in the normalized deposition rate is 3% using data from a separate simulation with the QMB shifted downward by 1 cm. The simulated QMB is assumed to point downward, although its precise orientation has not been measured. Because the number of collisions experienced by lithium atoms striking the QMB en route from the evaporator is of order unity ($\lambda_{\mathrm{Li-He}} = 0.33$ m at the highest pressure) and due to the presence of nearby solid structures (divertor and passive plate tiles), the code results are sensitive to this angle. Two simulations in which the QMB was tilted radially by 30° inward and outwards yielded an average deviation of 46% from the 0.25 mtorr baseline run; the actual angle of the QMB relative to horizontal is likely less than this. For simplicity, we combine these two uncertainties into a single figure of 25%.

The uncertainty in the location of the QMB within the gap between the surrounding plates is also estimated to be 1 cm, even though the width of the gap has been explicitly measured. In this case, the sensitivity of the normalized deposition rate can be found using data from adjacent toroidal segments in the simulations. An average deviation of 10% is found from the resulting data points.

The location of the LITERs in their operating position is not precisely known, even though the locations of points on the surrounding tiles has been measured. Two sensitivity simulations were carried out in which the LITERs were moved radially outward within this tile gap by 6 mm. The deposition rate in these simulations was

about 28% lower than in the baseline runs. Most of this drop is due to increased deposition (from 8% to 33% at 0.25 mtorr) on the backs and sides of the tiles adjacent to the LITERs.

The gas pressure and scattering cross sections both enter the problem only through the mean free path. Consequently, we can use the variation of the deposition rate with pressure (nearly linear, according to Fig. 4) to assess its sensitivity to the cross section. For these low interaction energies ($\ll$ 1 eV), resonances and other quantum effects introduce significant variations ($>$ 10%) in the momentum transfer cross sections [12] with small changes in the interaction energy. Quantum oscillations introduce even larger isotopic dependencies, up to 50%, in the case that a significant fraction of the out-gassing is H_2 or HD. We have also introduced errors by treating scattering of He and D_2 with a single cross section and ignoring angular dependence of the scattering. We account for all of these effects with a single uncertainty of 50%.

The relative fraction of He and D_2 in the vessel is not known and can only be estimated using the model described in Sec. 3.1. This translates into an uncertainty in the total pressure (the input to the simulations) since the measured quantity is the ionization gauge reading and not the total pressure. The ionization gauge calibration factors are such that variations in the assumptions used in that model lead to changes in the total pressure on the order of 40%.

A final, possibly significant, error may result from operating the LITERs at temperatures above 870 K. Under these conditions, the evaporated lithium in the LITER snout may no longer be in the molecular flow regime used to estimate the evaporation rate and compute the angular distribution of emitted atoms. The conductance of the snout in this case would be expected to increase strongly with the lithium vapor pressure, and consequently, with temperature. The corresponding enhancement in the evaporation rate beyond that predicted by the molecular flow formula could be a factor of two, or even more. Note that an increased evaporation rate would reduce the measured normalized deposition rate, exacerbating the disparity with the simulation results seen in Fig. 4. On the other hand, a departure from molecular flow might result in a more centrally peaked angular distribution for the atoms that would act in the other direction. Because of the magnitude and complexity of these considerations, we do not account for them in the remaining analysis.

The above uncertainties are all independent so that we can sum their squares to obtain a total error of 75% in the simulations. The error bars in Fig. 4 are actually $\sqrt{2/\pi}$ of this value, as is suggested by the validation metric in [13].

The experimental data were divided into 0.01 mtorr wide bins around the simulated pressure values; the resulting mean values are indicated by the upper ends of the rectangles plotted in Fig. 4. The lower ends are 7/24 of these rates, representing the

complete hydration of deposited lithium into LiOH. Note that the 90% confidence intervals described in [13] are much smaller than than the uncertainty introduced by the undetermined chemical composition of the QMB deposits and are not shown in Fig.4.

While the simulation error bars do overlap the experimental data rectangles, the consistent $\geq 50\%$ discrepancy between the simulated and the experimental rates, as well as the "tracks" apparent in the experimental data, suggest the presence of a hidden parameter or systematic error that needs to be identified. To this end, we plan dedicated experiments that will decouple the components of the model and assist us in improving it. For example, we can operate the LITERs separately, utilize QMBs in other parts of the vessel, and run the LITERs at lower temperatures to ensure the validity of the molecular flow assumption. The uncertainties can also be reduced with additional in-vessel measurements. The effects of out-gassing can be nearly eliminated by continuously pumping the vacuum vessel while maintaining the prescribed helium pressure via injection through a leak valve. A postmortem ex-vessel analysis of the QMB will allow the degree of hydration of the deposited lithium to be quantified.

5 Conclusions

In conclusion, we have developed a DEGAS 2 based model for predicting and optimizing the coating of the NSTX vessel with lithium via diffusive evaporation into a helium filled vessel. The results of the validation effort described here point to the most significant uncertainties in the model and suggest more discriminating validation experiments.

Acknowledgments

This work supported by U.S. DOE Contracts DE-AC02-09CH11466 and DE-AC05-00OR22725. The authors wish to thank C. Priniski for the in-vessel spatial calibration data used in this work and one of the reviewers for pointing out the possibly significant effects of water on these experiments. The authors would also like to acknowledge discussions on this latter point with R. Majeski, J. P. Allain, and M. Jaworski.

References

[1] M. Ono et al., Nucl. Fusion 40 (2000) 557.

[2] H. W. Kugel et al., Phys. Plasmas 15 (2008) 056118.

[3] R. Maingi et al., Phys. Rev. Lett. 103 (2009) 075001.

[4] M. G. Bell et al., Plasma Phys. Control. Fusion 51 (2009) 124054.

[5] C. H. Skinner et al., J. Nucl. Mater. 390–391 (2009) 1005.

[6] D. P. Stotler et al., J. Nucl. Mater. 290–293 (2001) 967.

[7] D. P. Stotler, T. D. Rognlien, S. I. Krasheninnikov, Phys. Plasmas 15 (2008) 058303.

[8] W. A. Hamel et al., J. Phys. B: At. Mol. Phys. 19 (1986) 4127.

[9] C. H. Skinner et al., Rev. Sci. Instrum. 75 (2004) 4213.

[10] C. H. Skinner et al., J. Nucl. Mater. 363–365 (2007) 247.

[11] C. N. Taylor et al., J. Nucl. Mater. (these proceedings).

[12] P. S. Krstic, D. R. Schultz, J. Phys. B: At. Mol. Opt. Phys. 42 (2009) 065207.

[13] P. W. Terry et al., Phys. Plasmas 15 (2008) 062503.

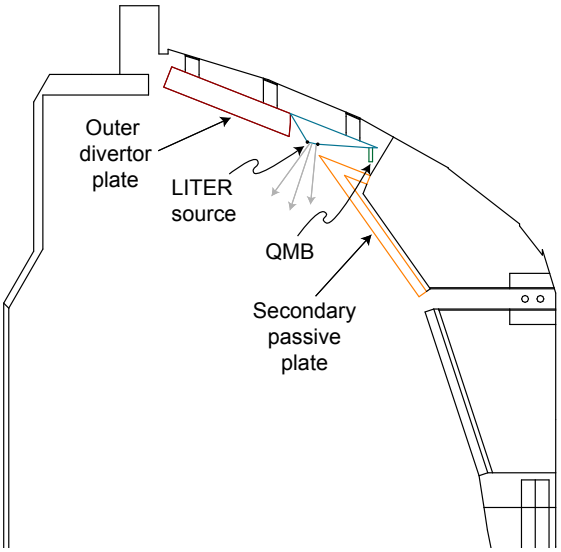

Figure 1. Poloidal plane figures used to construct the vacuum vessel elements in the model.

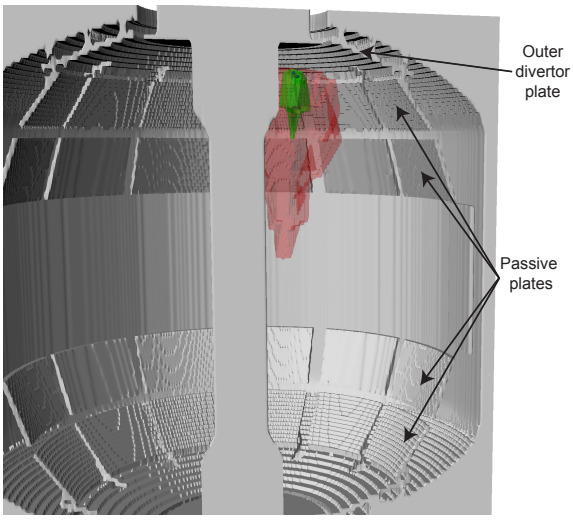

Figure 2. Three-dimensional rendering of the vacuum vessel elements in the model. Two lithium density contours associated with the Bay F LITER are also included. The apparent corrugation of the surfaces, especially the outer divertor plate, is an artifact of the method used to generate the plot and is not present in the computational model.

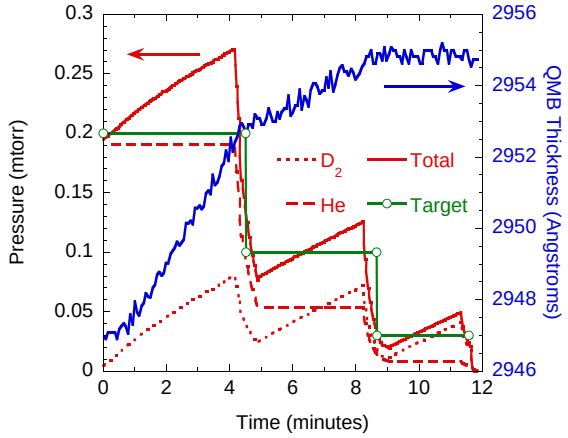

Figure 3. Pressure and QMB data from shot 135697. The "Target" points indicate the prescribed helium pressures. The actual helium, deuterium, and total pressures are inferred from the experimental ionization gauge data via the model described in Sec. 3.1. The corresponding QMB thickness data are overlaid (right axis).

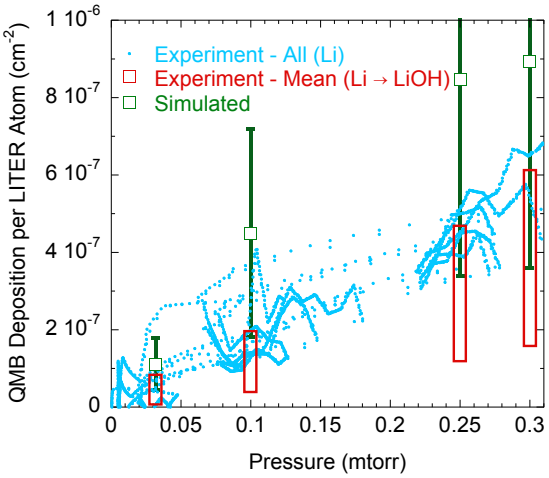

Figure 4. The deposition rate on the QMB, assumed to be pure lithium, normalized by the total LITER evaporation rate, is plotted as a function of the total (He and D_2) pressure. All of the experimental data are shown as small points. The upper ends of the open rectangles are the means of these data at the pressures used in the simulations; the lower ends represent the mean values obtained if the QMB deposit is assumed to be pure lithium hydroxide. The simulated data are plotted as open squares with error bars determined as described in the text.